DISCRETE ELEMENT METHOD USED TO ANALYZE THE OPERATING PARAMETERS OF THE CUTTING TABLE OF CRAWLER SELF-PROPELLED REED HARVESTER
/
离散元法分析履带自走式芦苇收获机割台运行参数

Kuizhou JI [1)], Yaoming LI [1*)], Binbin JI[1,2)], Zhenwei LIANG [1)], Tuo DU[1)]
[1)] School of Agricultural Engineering, Jiangsu University, Zhenjiang, 212013, China
[2)] School of Mechanical Engineering, Nantong University, Nantong, 226019, China
Tel: 13805283656; E-mail: ymli@ujs.edu.cn
Corresponding author: Yaoming Li
DOI: https://doi.org/10.35633/inmateh-71-30

Keywords: *Discrete element, reed combine harvester, cutting table, multiple factors*

ABSTRACT
In this paper, the basic rigid unit and discrete element rigid model of reed stem and discrete element flexible model of reed stem were established by means of multi-spherical filling and other methods. Then, three-point bending test was carried out in EDEM software to complete the calibration of bonding parameters. Finally, simulation analysis was carried out with the loss rate as the index. The simulation results show that the optimal parameter combination is 46 r/min for the transverse transmission device, 53 r/min for the vertical clamping longitudinal transmission device, and 470 mm for the center distance of the drum. Finally, the initial field test verifies that the maximum parameter combination of the harvester header is 49 r/min for the transverse conveying device of the header, 51 r/min for the vertical clamping longitudinal conveyor and 1.1 m/s for the field forward speed of the reed harvester, and the loss rate of the harvester is 3.36%, and the optimal parameter combination is consistent with the simulation analysis results.

摘要
本文通过多球面体填充等方法建立了芦苇茎秆的基本刚性单元与离散元刚性模型以及芦苇茎秆的离散元柔性模型，随后在 EDEM 软件中开展了三点弯曲试验，完成了粘结参数的标定，最后以损失率为指标开展仿真分析，仿真结果表明最佳参数组合为横向拨送装置转速为 46r/min、直立夹持纵向输送装置转速为 53r/min、滚筒中心距为 470mm，最后通过初次田间试验验证了履带自走式芦苇收获机割台收获效果最大的参数组合为割台横向拨送装置工作转速为 49r/min、直立夹持纵向输送装置工作转速为 51r/min 和芦苇收获机田间前进速度为 1.1m/s 时，此时收获机割台的损失率为 3.36%，最优参数组合与仿真分析结果相符.

INTRODUCTION

Transverse transfer and longitudinal clamping of the whole reed stalk are the key technologies of the cutting table of crawler self-propelled reed harvester, and the working performance of the corresponding device directly affects the reed loss rate *(Jin et al., 2010, Liu et al., 2021)*. The first section is transverse transfer. After the reed stalk root is cut off, the transverse transfer device is transferred to the front end of the vertical clamping longitudinal transfer device. The second section is longitudinal conveying. The reed stalk is transported from the front end to the rear binding mechanism by the vertical clamping longitudinal conveying device. The connection of the two sections of conveying device is realized by the finger of the transverse transmitting device and the conveying roller.

At present, there are reed harvesters at home and abroad, they choose silage harvester headers to cut the reeds, and then the square baler pulled by the tractor collects and bales the broken reeds and sends them to the trailer for storage *(Luigi et al., 2016). Martelli et al* attached a header in front of the tractor, which contains a grinder to cut and crush the reeds *(Martelli et al., 2015). Ivan et al* designed a reed harvester capable of harvesting reed vegetation located at the edge of canals and lakes, consisting mainly of a floating harvesting device, a platform for conveying and storing reeds *(Ivan et al., 2017).* Jiangsu Binhai County Agricultural Mechanization Institute is designed to be 4GL-130 reed harvester on the basis of rice and wheat harvester, which is compact in structure, easy to hook, and adopts vertical header and manual lifting (*Yuan et al., 1987*). Ma Qingyong discussed and studied the position of the reed cutter table, and used the tracked chassis to solve the problem of heavy load on the front wheel of the harvester (*Ma et al., 2010*).

Yuan Chunfu improved the header device of the reed harvester in view of the problem of small cutting width of the reed harvester, and its cutting mechanism was composed of three cutters, which were respectively responsible for the cutting of the roots of the high-stem crop, the root of the high-pole crop and the cutting of the rattan on the side of the cutting surface (*Yuan et al., 2014*). *Ni et al* designed the reed harvester for the phenomenon that it is prone to lodging and jamming in the reed harvest process. Therefore, the multi-layer conveying chain is used to push the reed wheel and the moving tooth to drive the reed to move in the rotating direction of the chain (*Ni et al., 2021*).

In order to transport reed stalks neatly and orderly from transverse to longitudinal, this paper uses EDEM software to conduct discrete element simulation research on reed stalk transport process of crawler self-propelled reed harvester, establishes the rigid and flexible discrete element model of reed stalk, and constructs the transportation system simulation system of reed stalk from transverse conveying mechanism to vertical clamping longitudinal conveying mechanism. Discrete element method has been widely used *(Wang et al., 2010, Andrewg et al., 2011).* This method can provide information about the macroscopic and microscopic behavior of the particle system. *Lv et al., (2023),* verified the operation performance of their designed potato soil crushing and preparation combined operator by establishing a component-soil discrete element model. *Zhou et al., (2023),* established the root-tuber of Jerusalem artichoke at harvest time and calibrated its physical characteristics, thus laying a research foundation for the harvester.

The discrete element rigid model of reed stems was established by means of EDEM software polyhedron filling and layering. The discrete element flexible model of reed stems was established by Hertz-Mindlin with bonding contact model, and the parameters were calibrated by three-point bending test. The simplified discrete element model of the transversal conveyance and the longitudinal clamped conveyance was established, and the optimal rotation speed was obtained by dynamic analysis, which provided a theoretical basis for the selection of parameters in the subsequent field operation.

MATERIALS AND METHODS

Crawler self-propelled reed harvester cutting table device overall scheme design

Cutting table design scheme

The cutting platform of reed harvester designed in this paper integrates the functions of cutting, transverse transfer and longitudinal clamping, and can achieve low loss and high efficiency harvesting of the whole reed rod. The reed harvester cutting table device is mainly composed of the left and right dividing rod, cutting device, transverse transfer device, vertical clamping longitudinal conveying device and other working parts. The 3 D map is shown in Figure 1 (a), the physical diagram is shown in Figure 1 (b).

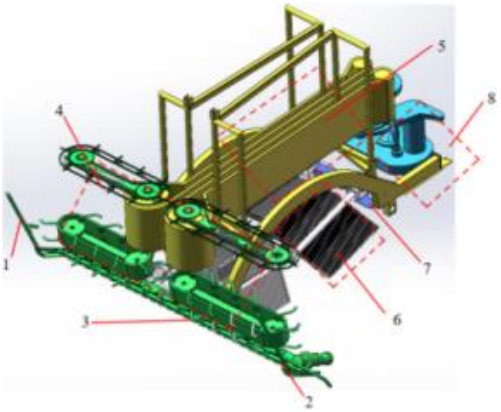

Fig. 1(a) - 3D illustration of header

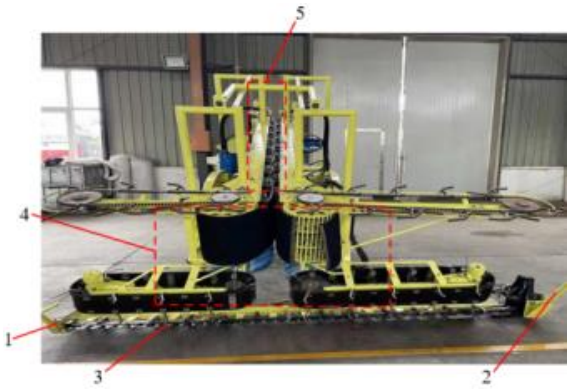

Fig. 1(b) - Real object of header

1-The right dividing rod of the cutting table; 2-cutting table left dividing rod; 3-cutting table cutting device; 4- cutting table transverse transfer device; 5-cutting table vertical clamping longitudinal conveying device; 6-cleaning device;7-bottom root device; 8-strapping device

Working principle of the cutting table device

When the crawler self-propelled reed harvester cutting platform device performs field harvesting operations, the hydraulic cylinder is responsible for controlling the lifting of the harvester cutting platform device, the reed plants are divided into ridges by the left and right dividers, and the reed plants are gathered and collected by the lateral transfer device. The reed stalks after cutting are transferred from both sides to the middle. The reed stalk is fed into the vertical clamping longitudinal conveying device by an active roller fitted with the high friction conveyor belt, and the reed stalk is finally transported by clamping at the entrance of the device to the binding place at the tail.

Discrete element analysis of transverse versus longitudinal conveying devices

Establishment of discrete element modeling

As shown in Fig.2, simplifying the three-dimensional model of the transverse and longitudinal gripper conveyer-device, leaving only the end of the transverse conveyer-device and the front end of the vertical gripper longitudinal conveyer-device affects the transition part of the tall reed stalk from the transverse conveyer-device to the longitudinal gripper conveyer-device.

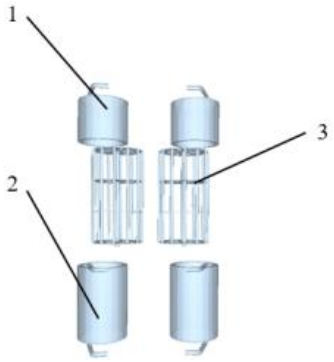

Fig. 2 - Simplified lateral and longitudinal conveying devices

1- Upper horizontal transfer mechanism; 2- Lower horizontal transfer mechanism; 3- Vertical clamping longitudinal conveyor

Definition of the reed stalk model

The Hertz-Mindlin with bonding contact model was used to construct the flexible model of reed culms *(Zhang et al., 2018).* The reed plants involved in this paper vary in length from 2.5-3 m and in diameter from 12-20 mm. In order to improve the simulation speed, the reed stalk model is simplified according to the physical characteristics of the reed stalk, and it is regarded as a hollow cylinder composed of rings composed of numerous particles and stacked with layers of rings. Basic parameters are shown in Table 1. It provides data basis for the establishment of reed stem discrete meta-model *(Bart et al., 2014).*

Table 1

Geometric dimensions of reed stalks

Parameter	Scope / mm	Mean value / mm
Culm length	2500~3000	2750
Stem wall thick	1.8~2.6	2.2
Stem diameter	12~20	16

Establishment of the Rigid model

The basic rigid element of reed stem was established by means of multi-spherical filling and layering *(Wang et al., 2020).* The specified particle coordinate rules (part) are shown in Fig.3 and Fig.4, and the discrete element rigid model of reed stalk established is shown in Fig.5.

	Position X (mm)	Position Y (mm)	Position Z (mm)	Physical Radius (mm)
4	2.03522	5.28128	-0.00130431	2.3
5	-5.27647	2.03485	-0.00184566	2.3
6	5.28165	-2.0304	0.000474478	2.3
7	-2.03004	-5.27683	-6.68751e-05	2.3

Fig. 3 - The polyhedron filling method

	Name	Particle Type	Position X (mm)	Position Y (mm)	Position Z (mm)
328	particle 337	New Particle 2	0	0	1546.3
329	particle 329	New Particle 2	0	0	1551
330	particle 330	New Particle 2	0	0	1555.7
331	particle 338	New Particle 2	0	0	1560.4
332	particle 339	New Particle 2	0	0	1565.1

Fig. 4 - Layered overlay method

Fig. 5 - Schematic diagram of discrete element rigid model of reed stalk

Establishment of the flexible model

In order to restore the deformation process of reed stems and improve the simulation accuracy, on the basis of the rigidity model of reed stems established by the multi-spherical filling method, the Hertz-Mindlin

with bonding contact model is used to bond each unit, and the force/moment between particles is set to 0 and updated gradually by Formula 1 *(Liu et al., 2018)*:

$$\begin{cases} \Delta F_{nb} = -v_n^{rel} k_{nb} A_b \Delta t \\ \Delta F_{tb} = -v_t^{rel} k_{tb} A_b \Delta t \\ \Delta M_{nb} = -\omega_n^{rel} k_{nb} J_b \Delta t \\ \Delta M_{tb} = -\omega_t^{rel} k_{tb} J_b \Delta t \end{cases} \quad (1)$$

The A_b cross-sectional area and polar moment of inertia J_b of parallel bonding bond are calculated as follows:

$$\begin{cases} A_b = \pi R_b^2 \\ J_b = \frac{1}{2}\pi R_b^4 \end{cases} \quad (2)$$

where ΔF_{nb} represents the increment of normal bonding force, [N], ΔF_{tb}represents tangential bonding force increment, [N], ΔM_{nb} increment of normal bonding moment is expressed, $[\mathrm{N \cdot m}]$, ΔM_{tb} represents tangential bonding moment increment, $[\mathrm{N \cdot m}]$, k_{nb} expresses normal bond stiffness, $[\mathrm{N/m^3}]$, k_{tb} denotes tangential bond stiffness, ω_n^{rel} represents the normal relative angular velocity, $[\mathrm{rad/s}]$, ω_t^{rel} tangential relative angular velocity, $[\mathrm{rad/s}]$, Δt indicating that the time is not long, [s], R_b denotes the bonding radius.

When the maximum normal stress σ_{max} and maximum tangential stress τ_{max} between particles exceed the predefined critical normal stress $\sigma_{critical}$ and critical tangential stress $\tau_{critical}$, the bonding bond between particles breaks:

$$\begin{cases} \sigma_{critical} < \sigma_{\max} = \frac{-F_{nb}}{A_b} + \frac{2M_{tb}}{J_b} R_b \\ \tau_{critical} < \tau_{\max} = \frac{-F_{tb}}{A_b} + \frac{2M_{nb}}{J_b} R_b \end{cases} \quad (3)$$

where F_{nb} represents the normal bonding force, $[N]$, F_{tb} represents the tangential bonding force, $[N]$, M_{nb} represents the normal bonding moment, $[\mathrm{N \cdot m}]$, M_{tb} Represents the tangential bond moment, $[\mathrm{N \cdot m}]$.

The state of reeds harvested by reed harvester can be judged by observing the stress of stalk model and the state of bonding bond.

Calibration of the bonding parameters

It is necessary to determine material parameters (density and Poisson's ratio, etc.), contact parameters (recovery coefficient and static friction coefficient, etc.) and bonding parameters (normal and tangential bonding parameters, etc.), and to calibrate the normal bonding strength k_n, tangential bonding strength k_s and radius between reed stalk particles by three-point bending test *(Gonzalez, et al., 2012; Hou et al., 2022).*

Three-point bending test

As shown in Figure 6, the geometric model of the support seat and indenter is established in EDEM software, and a force of 5N downward movement is applied to the indenter, and the loading speed is 10 mm/min. The time step is 5%, and the mesh is 3 times the particle *(Tong et al., 2022; Yidong et al., 2023).*

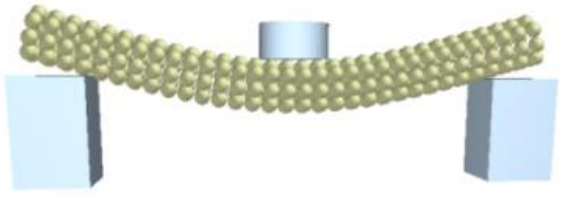

Fig. 6 - Three-point bending test in EDEM software

As shown in Table 2 and 3, the specific values of material parameters and contact parameters are given by referring to literature, and the bonding parameters mainly include: normal bonding strength, tangential bonding strength, bonding radius, critical normal stress and critical tangential stress.

Table2

Reed material parameters

Material	density（$\mathbf{kg \cdot m^{-3}}$）	Poisson ratio	Modulus of shearing（Pa）
Reed stalk	200	0.5	$4x10^6$
Loading parts	7800	0.3	$8x10^{10}$

Table3

Reed material parameters

Material	Recovery coefficient	Static friction coefficient	Sliding coefficient
Reed stalk-reed stalk	0.284	0.3	0.20
Reed stalk-Load piece	0.43	0.250	0.122

Test protocol and results

The test method of Box-Behnken using Design-Expert software, using the normal bond strength k_n, intensity of tangential bonding k_s and adhesion radius r as the test factors, and the bending strength as the test index. The test code is shown in Table 4:

Table4

Three-point bending test code list

Factor	Level		
	-1	0	1
Normal bond strength（N/m^3）	10^6	10^9	10^{12}
Intensity of tangential bonding （N/m^3）	10^6	10^9	10^{12}
Adhesion radius（mm）	1	3	5

The test index is the bending strength of reed stalk, and the calculation formula is as formula (4):

$$\delta_l = M_{\max} / W \tag{4}$$

where δ_l represents the bending strength of reed, [MPa], M_{max} represents the maximum bending moment, $[\mathrm{kNm}]$, W represents the cross-section coefficient, the cross section of reed stalk is:

$$W = \frac{\pi\varphi^3}{32}\left[1-\left(\frac{d}{\varphi}\right)^4\right] \tag{5}$$

where φ^3 represents the cross-section diameter of the reed stalk and d represents the inner diameter of the reed stalk. Three-factor three-level test performed using the Box-Behnken design test method of Design-Expert software. The results are shown in Table 5:

Table5

Analysis of three-point bending test results

Order	A: Normal bond	B: Intensity of tangential	C: Adhesion	δ_l（MPa）
1	1	0	-1	9.45
2	0	1	1	17.56
3	-1	0	-1	0.71
4	1	0	1	15.61
5	0	0	0	2.35
6	1	-1	0	5.41
7	0	-1	-1	1.44
8	1	1	0	18.62
9	0	0	0	2.37
10	0	0	0	2.39
11	0	0	0	2.38
12	0	-1	1	8.12
13	-1	1	0	7.62
14	0	1	-1	12.45
15	0	0	0	3.38
16	-1	0	1	6.44
17	-1	-1	0	0.35

The above results were fitted by quadratic polynomial regression, and the second-order regression model of the bending strength of reed stems, the normal and tangential bond strength and the bond radius was established, and the analysis of variance was carried out, as shown in Table 6.

Table 6

Analysis of variance of three-point bending test results

1	quadratic sum	free degree	free degree	F price	P price
model	572.75	9	63.64	358.65	<0.0001
A-k_n	144.25	1	144.25	812.91	<0.0001
B-k_s	209.41	1	209.41	1180.15	<0.0001
C-r	70.09	1	70.09	395.02	<0.0001
AB	8.82	1	8.82	49.71	0.0002
AC	0.046	1	0.046	0.26	0.6255
BC	0.62	1	0.62	3.47	0.1047
A^2	13.54	1	13.54	76.29	<0.0001
B^2	55.57	1	55.57	313.19	<0.0001
C^2	57.19	1	57.19	322.31	<0.0001
Residual	1.24	7	0.18		
Lack of Fit	0.43	3	0.14	0.70	0.5975
Pure Error	0.81	4	0.20		
Cor Total	573.99	16			

It can be obtained from the table that the model *P* value of the regression model 0.0001, and then it is known that the model is extremely significant. However, the P-value of the mismatch term was 0.5975> 0.005, which was not significant, indicating that the regression model fitted more reliably. The results of variance analysis show that the regression model of flexural strength of reed stems is reliable and can be used to predict flexural strength of flexible reed stems.

The regression equation of the regression model is as follows:

$$\delta = 2.57 + 4.25A + 5.12B + 2.96C + 1.48AB + 0.11AC - 0.39BC + 1.79A^2 + 3.63B^2 + 3.69C^2 \quad (1)$$

Using Design Expert software to solve the above model with the initial design point as the starting point, the optimal parameter combination of normal bond parameters, tangential bond parameters and bond radius can be obtained as follows:

1) The normal bond strength is 8.5×108 $\mathrm{N/m^3}$; 2) Tangential bond strength is 6.5×107 $\mathrm{N/m^3}$; 3) The bonding radius is 2.6 mm.

The three-point bending test was carried out again with the above parameter combination, and the bending strength of the reed stem was 2.43 MPa, which was 6.18% lower than that measured by the texture analyzer above (2.59 MPa), proving that the best parameter combination obtained can be used to establish the flexible reed stem model.

RESULTS

Experimental factors and indexes

This test mainly selects three main factors: the rotational speed of the transverse device, the vertical clamping speed and the center distance of the roller. The main evaluation index of the experiment was the loss rate of the transported reed stalk. In the EDEM software, Bond Status can determine whether the reed stalk has broken. As shown in Figure 7, the whole reed stalk is connected into a whole.

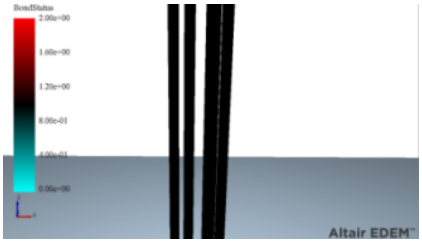

Fig. 7 – Bond Status of flexible reed stalks during EDEM analysis

Test protocol design

In this paper, Box-Behnken method was used to establish a mathematical model between the three factors of the transverse transfer device speed, the lower conveying speed and the active drum speed and the two evaluation indexes of reed stem loss rate, and the optimal parameter combination and the optimal response value were analyzed and found out. The test code table is shown in Table 7:

Table 7

Code list of discrete element simulation test of horizontal transfer and longitudinal clamping conveying device

Factor	Level		
	-1	0	1
A: The center distance of the drum (mm)	400	500	600
B: Transverse conveyor speed (r/min)	30	50	70
C: Upright clamping longitudinal conveyor speed (r/min)	30	50	70

A three-factor and three-level orthogonal test scheme was adopted in the experiment. The center distance of the drum A, the speed of the transverse transfer device B and the speed of the vertical clamping longitudinal transport device C were selected as the test factors. The loss rate of the flexible discrete element model of reed stalk was used as the test index.

Simulation sand analysis

As shown in Figure 8, at the beginning of the simulation, the particle factory generated a flexible reed stalk near the tooth, and the reed stalk continuously accelerated downward movement. Then move from both sides to the center. When the teeth move to the center position, the flexible reed stalk is transferred to the gripper conveyor belt behind the conveyor drum.

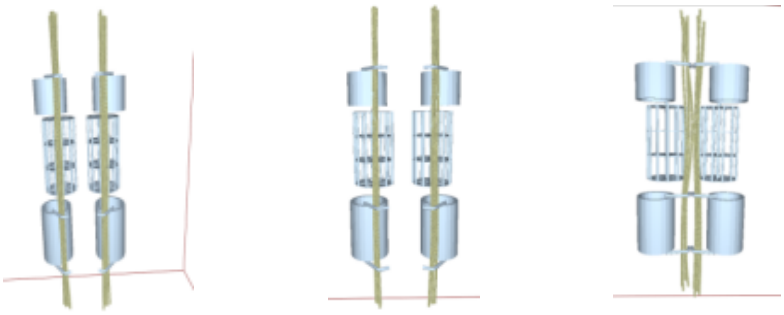

Fig. 8 - Simulation process analysis of transporting reed stalks with a device

Fig. 9 – Bond Status of flexible reed stalks during simulation

(a) Bond Status when there is no breakage (b) Bond Status when there is breakage

As shown in Figure 9 (a), when the reed stem is not in contact with the picking teeth, one rigid reed stem unit is bonded together by a bonding bond. When the reed stem is subjected to external forces, the surface of the reed stem skin will maintain a stable shape, which can effectively reduce the damage of external forces on the reed stem.

As shown in Figure 9 (b), when the flexible reed straw is too stressed in instantaneous time, the bond will be completely disconnected, and each rigid reed unit spreads under the influence of gravity. At this time, the reed straw is broken.

Analysis of the simulation results

In this test, the three-factor and three-level test protocol design was conducted by using the Box-Behnken test design method in Design-Expert *(Tumuluru et al., 2023)*. The response surface test protocol and results are shown in Table 8.

Table 8

Simulation analysis of transverse transfer and vertical clamping conveying process

Order number	A (mm)	B (r/min)	C (r/min)	Loss rate R (%)
1	1	0	1	5.9
2	0	1	1	7.2
3	0	0	0	4.8
4	1	0	-1	7.4
5	0	1	-1	7.8
6	0	-1	1	6.6
7	0	-1	-1	6.3
8	0	0	0	4.9
9	-1	-1	0	6.6
10	0	0	0	5.1
11	-1	0	-1	5.8
12	1	1	0	8.2
13	1	-1	0	6.8
14	0	0	0	5
15	-1	1	0	7
16	0	0	0	4.8
17	-1	0	1	5.6

Using Design-Expert software to fit the above results, the second-order regression model of the lateral transmission device speed, the vertical clip speed and the center distance of the roller was analyzed by variance, and obtained the results as shown in Table 9.

Table 9

Analysis of variance of simulation results

1	quadratic sum	free degree	mean square	F value	P value
model	18.84	9	2.09	41.21	<0.0001
A	1.36	1	1.36	26.80	0.0013
B	1.90	1	1.90	37.44	0.0005
C	0.50	1	0.50	9.85	0.0164
AB	0.25	1	0.25	4.92	0.0620
AC	0.42	1	0.42	8.32	0.0235
BC	0.20	1	0.20	3.99	0.0860
A2	2.15	1	2.15	42.38	0.0003
B2	9.66	1	9.66	190.29	<0.0001
C2	1.23	1	1.23	24.18	0.0017
Residual	0.36	7	0.051		
Lack of Fit	0.29	3	0.096	5.64	0.0641
Pure Error	0.068	4	0.017		
Cor Total	19.19	16			

From Table 9, the P value of the regression model =0.0001 <0.05, and the model is extremely significant, while the misfit term is 0.0641> 0.005, indicating a high degree of fit. The results of ANOVA showed that the regression model of reed stalk has high confidence in the prediction of flexible reed stalk.

The regression equation for this regression model is:

$$R=4.92+0.41A+0.49B-0.25C+0.25AB-0.33AC-0.22BC+0.71A^2+1.52B^2+0.54C^2 \quad (2)$$

Field testing

In order to verify the effect of crawler self-propelled reed harvester, this paper conducted a preliminary field test. In the field test map shown in Figure 10, the reed harvesting function was successfully divided, and there were few unharvested reed stalks in the process of dialing, and the whole cutting table device was not stuck or blocked. The best parameter combination of the test results is shown in Table 10.

Fig. 10 - Field test of crawler self-propelled reed harvester header

Table 9

Optimum parameter combination for the test results

Parameter	Optimal working speed of the header transverse toggle device (r/min)	The cutter holds the optimal longitudinal conveyor speed (r/min)	Minimum loss rate
value	49	51	3.6%

DISCUSSION

Figure 11 shows the response surface of the speed B of the transverse transfer device and the speed C of the vertical clamping longitudinal transfer device to the loss rate R when the center distance of the cylinder A is 500 mm. It can be seen from the figure that when the speed of the transverse transmission device B is fixed, under the speed condition of 30 ~ 42 r/min, the loss rate R decreases significantly with the increase of the speed of the vertical clamping longitudinal transmission device C, and maintains a low loss rate between 42 ~ 64 r/min, and then the loss rate rises slowly. When the vertical clamping longitudinal conveying device C is fixed, under the speed condition of 30 ~ 42 r/min, the loss rate R decreases significantly with the increase of the transverse transmitting device speed B, and maintains a low loss rate in 42 ~ 52 r/min, and then the loss rate rises slowly. It can also be seen from the figure that the influence of the speed of the transverse transfer device B on the loss rate is more significant than that of the vertical clamping longitudinal transmission device C.

Figure 12 shows the response surface of the cylinder center distance A and the vertical clamping longitudinal conveying device C to the loss rate R when the rotating speed of the transverse transfer device B is 50 r/min. It can be seen from the figure that when the center distance of the cylinder A is fixed, the loss rate R decreases significantly with the increase of the speed of the vertical clamping longitudinal conveying device C at the speed of 30 ~ 42 r/min, and maintains a low loss rate at 42 ~ 64 r/min, and then the loss rate slowly rises. When the speed of vertical clamping longitudinal conveying device C is fixed, the loss rate R increases significantly with the increase of the distance between the center of the cylinder and A under the condition of 400 ~ 420 mm, and maintains a low loss rate between 400 ~ 420 mm, and then the loss rate increases slowly. It is obvious from the figure that the impact of cylinder center distance A on the loss rate is more significant than that of the vertical clamping longitudinal conveying device speed C.

Figure 13 shows the response surface of the cylinder center distance A and the transverse transfer device speed B to the loss rate R when the speed of the vertical clamping longitudinal conveying device C is 50 r/min. As can be seen from the figure, when the center distance of the cylinder A is fixed, under the condition of 30 ~ 42 r/min, the loss rate R decreases significantly with the increase of the speed B of the transverse transmission device, and maintains a low loss rate between 42 ~ 52 r/min, and then the loss rate rises slowly. When the transverse transfer device B is fixed, the loss rate R increases significantly with the increase of the speed of the cylinder center distance from A at the speed of 400 ~ 430 mm, and maintains a low loss rate at 430 ~ 520 mm, and then the loss rate slowly rises. It can be seen from the figure that the impact of the loss rate R on the center distance of the cylinder A is more significant than that on the center distance of the cylinder.

In the experiment, the working speed of the transverse transfer device of the cutting table is 49 r/min, the working speed of the vertical clamping device of the cutting table is 51 r/min, and the field advance speed of the harvester is 1.1 m/s, which is consistent with the simulation analysis results in this paper. Finally, the reed harvester conducted field tests again to verify this parameter combination, and the loss rate of the reed

harvester cutting table device was measured to be about 3.6%, which verified the reliability of the parameter combination, and also verified that the crawler self-propelled reed harvester cutting table device designed in this paper can harvest reed crops with low loss and high efficiency.

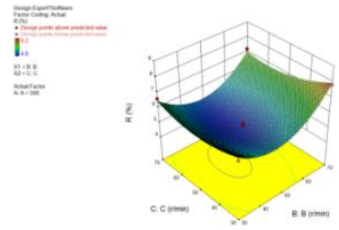

Fig. 11 - Influence of B and C on R when A is 500 mm

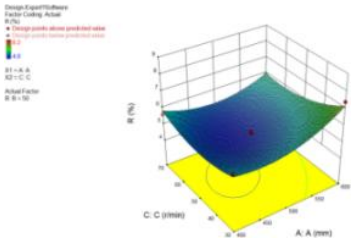

Fig. 12 - Influence of B and C on R when A is 500 mm

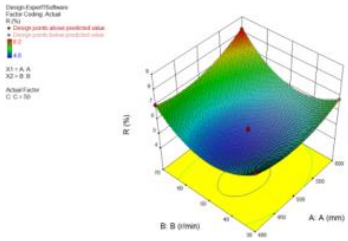

Fig. 13 - When C is 50 r/min, the influence of A and B on R

CONCLUSIONS

In this paper, the discrete element method was used to test the working speed of the transverse conveying device of the header, the working speed of the vertical clamping longitudinal conveyor and the field forward speed of the harvester, and the loss rate of the header of the reed harvester was used as the test index. The Box-Behnken orthogonal test method is used to establish the mathematical model of the above factors and indicators, and the optimal combination of parameters is obtained by multi-factor response surface analysis, and the specific conclusions are as follows:

(1) The basic rigid element and discrete element rigid model of reed stem were established by the method of multi-sphere filling and layering.

(2) Then the rigid flexible element is bonded into flexible element by Hertz-Mindlin with bonding contact model, and the discrete element flexible model of reed stalk is established.

(3) Then, a three-point bending test was carried out in EDEM software to complete the calibration of bond parameters necessary for the establishment of discrete element flexible model of reed stalk.

(4) The simulation results show that the optimal parameter combination is 46 r/min for the rotating speed of the transversal transmission device. The rotational speed of the vertical clamping longitudinal conveying device is 53 r/min. The center distance of the rollers is 470 mm.

(5) The results of the field test show that the working speed of the transverse transfer device of the cutting table is 49 r/min, the working speed of the vertical clamping device of the cutting table is 51 r/min, and the field advance speed of the harvester is 1.1 m/s. The optimal parameter combination is not much different from the simulation results in this paper. Finally, the reed harvester conducted field tests again to verify this parameter combination, and the loss rate of the reed harvester cutting table device was measured to be about 3.6%, which verified the reliability of the parameter combination, and also verified that the crawler self-propelled reed harvester cutting table device designed in this paper can harvest high-stalk reed crops efficiently. Due to time and environmental reasons, this paper has made a preliminary test of the reed harvester, but the feasibility of the scheme has been verified. In the future, this paper will continue to test, and further improve the performance of the harvester.

ACKNOWLEDGEMENT

This study was supported by the 2019 Jiangsu Provincial Science and Technology Plan Project (Key Project) (BE2019360), and each author helped me in my paper and experiment.

REFERENCES

[1] Andrewg, P., (2011). Development and validation of calibration methods for discrete element modelling. *Granular Matter*, Vol. 13(2), pp.127-132, America.

[2] Bart, L., Engelbert, T., Bart, D., Herman, R., Josse, D., & Wouter, S., (2014). Simulation of grain-straw separation by discrete element modeling with bendable straw particles. *Computers and Electronics in Agriculture*, Vol. 101, pp. 24-33, England.

[3] Ivan G., Ciupeca R., & Moise V., (2017). Kinematic scheme of equipment to reed harvesting machine MRS. *Engineering for Rural Development*, vol. 05, pp. 24-26, Latvia.

[4] Gonzalez, M., Fuentes, J., Ayuga, T., (2012). Determination of the mechanical properties of maize grains and olives required for use in DEM simulations. *Journal of Food Engineering*, Vol. 111(4), pp. 553-562, American.

[5] Hou, J., Xie, F., Wang, X., Liu, D., & Chen, Z., (2022). Determination of physical parameters of rice stalk contact and simulation calibration of discrete elements (水稻茎秆接触物理参数测定与离散元仿真标定). *Journal of Jiangxi Agricultural University*, Vol. 44(03), pp. 747-758, Jiangxi/China.

[6] Jin, J., (2014). Design and research of key components of reed harvesting vessels (芦苇收割船关键部件的设计与研究). *Agricultural University of Hebei*, Hebei/China.

[7] Liu, F., (2018). Discrete element modeling of wheat particles and short stalks in the cleaning device (清选装置中小麦颗粒和短茎秆离散元建模研究). *Northwest A & F University*, Shanxi/China.

[8] Lv, J., Liu, J., Zhao, Z., Yang, D., Li, J., & Sun, Q., (2023). Design and test of combined potato crusher and soil preparation machine (马铃薯碎土整地联合作业机设计与试验). *Journal of Agricultural Machinery*, Vol. 54 (08), pp. 19-29, Beijing/China.

[9] Luigi, P., Maria, D., Javier, S., (2016). Economic and energy analysis of different systems for giant reed. *Industrial Crops and Products*, Vol. 84, pp. 176-188, Holland.

[10] Liu, Y., (2021). *Design and testing of key components of chain cutting table for oil sunflower combine harvester (油向日葵联合收割机链切台关键部件的设计与试验). Huazhong Agricultural University*, Hubei/China.

[11] Ma, Q., Tian, L., & Wu, X., (2010). Design of 4WS2000 high pole reed harvester cutter table 4WS2000 (高杆芦苇收割机割台的设计). *Journal of Central South University of Forestry and Technology*, vol.30 (10), pp. 138-142, Han/China.

[12] Ni, Z., Ni, S., & Shen, Y., (2021). An elevated reed harvesting and baling device. CN214046684U, Jian gsu /China.

[13] Martelli R., Bentini M., Monti A., (2015). Harvest storage and handling of round and square bales of giant reed and switch grass, an economic and technical evaluation. *Biomass and bioenergy*, Vol. 83, pp. 551-558, England.

[14] Tumuluru, S., Armijo, B., Whitelock, P., (2023). Modeling and Optimization of High-Capacity Experimental Reclaimers to Minimize the Seed and Lint Loss during Roller Ginning of Upland and Pima Cotton. *Processes*, Vol. 11(10), pp.2868, Switzerland.

[15] Tong, S., Shao, M., Cao, M., & Zhao, J., (2023). Parameter calibration of corn stalk discrete element model based on DEM (基于 DEM 的玉米秸秆离散元模型参数标定). *China Agricultural Machinery and Chemical News*, 44(02), 69-75. Nanjing/China.

[16] Wang, G., Hao, W., Wang J., (2010). *Discrete cell method and its practice on EDEM (离散单元法及其在 EDEM 上的实践)*. Xian Polytechnic University Press, Xian/China.

[17] Wang, W., Liu, W., Yuan, L., Qu, Z., He, X., & Lv, Y., (2020). Wheat plant modeling and single longitudinal axial flow material movement simulation and experiment (小麦植株建模与单纵轴流物料运动仿真与试验). *Journal of Agricultural Machinery*, Vol. 51(S2), pp. 170-180, Beijing/China.

[18] Yuan, C., (2014). *High-rod crop harvester*. CN102652475B. Hunan /China.

[19] Yidong, X., Jordan, K., Tiasha, B., (2023). An experiment-informed discrete element modelling study of knife milling for flexural biomass feedstocks. *Biosystems Engineering*, Vol. 236, pp. 39-53, England.

[20] Yuan, W., Kuang, H., (1987) Type 4GL-130 reed harvester. *Agricultural machinery*, vol. 08, pp.17. Beijing/China.

[21] Zhou, J., Sun, W., Liang, Z., (2023). Construction of discrete flexible model during harvest (收获期菊芋根-块茎离散元柔性模型构建研究). *Journal of Agricultural Machinery*, Vol. 5, pp.1-16, Beijing/China.

[22] Zhang, T., Liu, F., Zhao, M., Ma, G., Wang, W., Fan, Q., & Yan, P., (2018). Measurement of contact physical parameters of corn stalk and discrete element simulation calibration (*玉米秸秆接触物理参数测定与离散元仿真标定*). *Journal of China Agricultural University*, Vol. 23(04), pp.120-127, Beijing/China.